The Dynamics of Dwarf Elliptical Galaxies

H. DEJONGHE[1] , S. DE RIJCKE[1], W. W. ZEILINGER[2], G. K. T. HAU[3]

[1]Sterrenkundig Observatorium, Ghent University, Belgium;
[2]Institut für Astronomie, University of Vienna, Austria; [3]ESO, Santiago, Chile

A short history

Dwarf elliptical galaxies (dEs) are small diffuse galaxies with smooth elliptical isophotes. One of the most nearby examples is NGC 205 (M110), a satellite of the Andromeda galaxy. From the days of the great comet-hunter Charles Messier up to well into the 20th century, this was the only known object of the class that we now call dEs. In 1944, Walter Baade confirmed NGC 147 and NGC 185 as members of the Local Group by resolving them into individual stars, a feat which was only possible because these dEs are very nearby galaxies. No new Local Group dEs have been discovered since then. In the 1950s, dEs were also discovered in the nearby Fornax and Virgo clusters, offering the possibility to study their photometric properties on larger samples: a dE is a rather gregarious species, spotted abundantly in dense environments such as clusters and groups of galaxies. Spectroscopy of such low-surface-brightness galaxies is challenging however, and had to wait until the early 1990s. At that time, 4 m-class telescopes, CCD cameras, in combination with long exposure times, could start to explore the kinematics and stellar populations of the central regions. Only now however, with large telescopes such as the VLT, do astronomers have the possibility to obtain spectroscopic information out to large radii, opening up the study of the spatial variations of the stellar populations and the determination of the orbital structure and dark matter content of dEs.

Models for dE Evolution

Although similar to normal ellipticals (Es) at first sight, dEs are quite different from their larger brethren. To begin with, dEs are much more diffuse objects with exponentially declining surface-brightness profiles (Es on the contrary are well described by the more centrally concentrated de Vaucouleurs law). Moreover, and again contrary to Es, dEs become noticeably redder towards larger radii. Current paradigm has it that star-formation proceeded most vigorously in the dense centres of Es, leading to a central population of metal-rich stars. These have many strong absorption lines in the blue part of the spectrum and thus make the centres of Es appear reddish. Finally, up to recent times, most of the dEs for which kinematic information was available turned out to rotate very slowly if at all. This sets them apart from the low-luminosity Es that are generally fast-rotating objects. This is the so-called "kinematic dichotomy" between Es and dEs. Wrapping this up, the photometric and kinematic differences between dEs and Es make it unlikely that ellipticals and dEs share a common origin or a similar evolution. Two currently popular models attempt to explain the properties of dEs (see Figure 1).

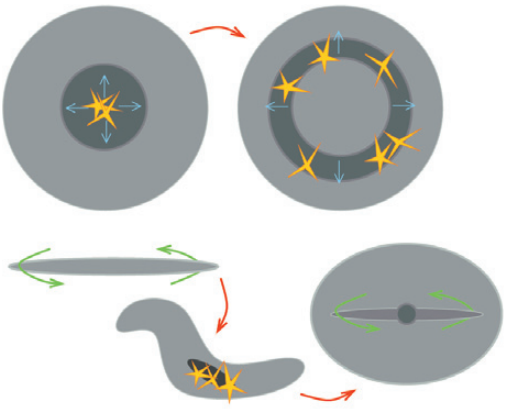

Figure 1: dE formation scenarios. Top : the wind-model. Supernovae blow away a dense gas shell (blue arrows) in which new stars are born. Subsequent supernovae further accelerate the shell and enrich it with metals. Bottom : the harassment scenario. A dE is initially a fast rotating (green arrows) small disc galaxy, destabilized by gravitational interactions. A bar develops and the disc is vertically heated. After a new equilibrium has been reached, the galaxy has a much rounder shape and slower (but still significant) rotation. Some relics of its previous state, e.g. a stellar disc, might survive the turmoil.

According to the **wind model**, dEs are primordial objects that formed from average-amplitude cosmological density fluctuations. Supernova explosions heat the interstellar medium (ISM) to velocities exceeding the galaxy's escape velocity and cause a supersonic outflow of gas from the galaxy, blowing away most, if not all, of the ISM. Stars form in this expanding shell and subsequent supernova explosions further accelerate its expansion and enrich it with metals. Since star-formation is enhanced at larger radii, dEs are more diffuse than Es (which have higher escape velocities and hold on to their gas more strongly) and have higher metallicities at larger radii, explaining the observed outward reddening of dEs. Since the stars are born out of gas that is moving outwards, the orbital distribution of the stars will favor radial orbits and rotation will be slow. There is a problem with this model however: standard cosmological models predict that small density fluctuations are less clustered than larger ones, from which the Es grow, contrary to the observed clustering properties of dEs.

The **harassment model** explicitly takes into account the fact that dEs are very clustered objects. N-body simulations have shown how a late-type (Sc-Sd) disc galaxy that orbits in a cluster or around a massive galaxy can be destabilized by gravitational interactions. The small disc galaxy develops a bar that transports angular momentum to the halo and to stars at larger radii which are lost as tidal tails. Gas is funneled in towards the centre by torques exerted by the bar where it is converted into stars, forming a nucleus. The originally rotationally flattened disc galaxy is heated and transformed into an anisotropic, slower rotating dE. The way a dwarf galaxy is affected depends on its orbit and some dEs may still contain some memory of their disky origin. Thus, these simulations not only offer a natural explanation for the clustering properties of dEs and the central luminosity spike (or "nucleus") observed in many bright dEs, but they also accomodate a number of recently discovered key observational facts: the existence of fast-rotating dwarfs, dEs that still contain gas and dEs with an embedded stellar disc.

An ESO Large Programme

We embarked on a Large Programme to obtain deep, high resolution spectra along the major and minor axis from a varied and sizeable sample of group and cluster dEs to study their internal dynamics and stellar populations. The goals of this program are (1) to assemble a large, homogeneous data-set of photometry, kinematics and dynamics of dEs of unprecedented high quality, (2) to model the dynamics of dEs ranging from dE0 to dE6, including dS0s, to check whether the kinematic dichotomy between Es and dEs is real and whether dEs become more rotationally

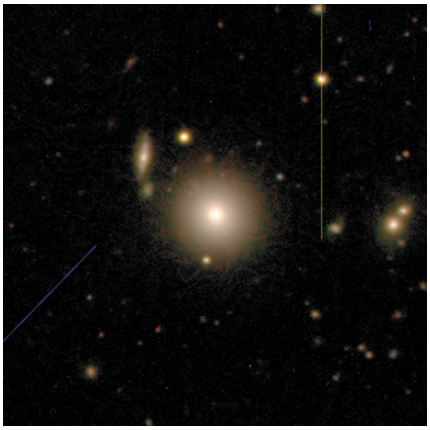

Figure 2: A VRI *color composite image of FS76, a NGC5044-Group dE1. North is up, east is to the left.*

supported as one goes to more flattened specimens, (3) to check the relation between the mass-to-light ratio and luminosity predicted by the wind model and whether a cuspy dark-matter density is required to fit the kinematic data (thus, dynamical models serve as a check on CDM cosmological models of galaxy formation), (4) search for dEs with peculiarities such as embedded discs, fast rotation, ionised gas, kinematically decoupled cores... that would support the harassment scenario, (5) measure line-strengths in the wavelength region λλ790–930 nm in order to study the stellar populations of the sample dEs.

We used FORS2, equipped with the very efficient volume phased holographic grating GRIS_1028z+29. This combination gives both a high throughput and high spectral resolution (σ_{instr} = 30 km/s with a 0.70″ wide slit), allowing us to accurately measure velocity dispersions as low as 20 km/s, which we verified by extensive Monte Carlo simulations. The exposure times were fine-tuned so as to reach 1.5–2 R_e with a signal to noise ratio S/N ≈ 15 per bin for the brightest dEs of our sample ($15 < m_B < 16$). For fainter objects ($m_B \geq 16.5$), we go out to 1–1.5 R_e at the same noise level. The standard data reduction procedures were performed with ESO-MIDAS. The individual spectra were bias-subtracted and flat-fielded. Cosmic ray events were removed and the spectra were binned to a linear wavelength scale (rectifying the emission lines of the arc spectra to an accuracy of 1 km/s FWHM). The sky background was subtracted very carefully. Using blank sky-spectra we corrected the spectra for variations of the slit-transfer function which resulted in a perfectly flat sky background that could be removed very accurately. The ubiquitous bright OH Meinel emission bands are undersampled at the high spectral resolution we are working at and proved much harder to remove completely. Fortunately, only a few galaxies had absorption lines that were affected by these emission lines. Finally, the spectra were flux-calibrated and co-added.

In the following, we will discuss the extraction of kinematic information from galaxy spectra and our dynamical modeling method, and present our results so far (De Rijcke et al. 2001, 2003a, 2003b).

Determining kinematics

The absorption lines in a galaxy spectrum are Doppler broadened due to the motions of the stars along the line of sight and their precise shape depends on the line-of-sight velocity distribution (LOSVD) of the stars. The LOSVD is approximated as a fourth-order Gauss-Hermite series, condensing the kinematic information to the mean velocity v_p, the velocity dispersion σ_p and two coefficients, h_3 and h_4, that quantify respectively asymmetric and symmetric deviations from a Gaussian LOSVD. These kinematic parameters can be obtained by fitting a weighted sum of stellar spectra, broadened with a parameterized LOSVD, to a galaxy spectrum. Doing this for each row of the galaxy spectrum yields the kinematics as a function of position along the slit.

Dynamical modeling

Kinematics along major and minor axis can be used to constrain the dynamics of a galaxy. A dynamical model consists of a gravitational potential and a distribution function. The potential generates the gravitational forces that bind the stars together, including the effects of the dark matter. The distribution function gives the number of stars on each orbit. From these two ingredients, all properties of a model can be calculated and compared to the observations. With our modeling technique, three-integral axisymmetric models are fitted to the kinematics. Since each model is given an absolute likelihood, a range of mass distributions that are compatible to the data at a given confidence level can be determined for each galaxy. This gives us detailed information about the orbital structures of the observed galaxies and allows robust estimates of their masses and mass-to-light ratios to be made.

FS76, a rotationally flattened dE

The non-nucleated NGC5044-Group dE1 FS76 (M_B=–16.70 for H_0=75 km/s/Mpc) is a case study of a rotationally flattened dE (De Rijcke et al. 2001). Our observations were carried out in May, 2000 with FORS2 on Kueyen. Total integration time was 5 h for each position angle. The analysis of the surface photometry confirms the picture of FS76 as a normal dwarf elliptical (see Figure 2). No photometric peculiarities were noted: there is only a modest amount of isophote twist; also no significant deviations from ellipses were detected in the isophotes. Its heliocentric velocity, derived from the spectra, confirms FS76 as a member of the NGC5044 group.

The central velocity dispersion σ_p equals 46 ± 2 km/s. The maximum rotation velocity along the major axis is 15 ± 6 km/s. The asymmetry in the mean velocity and velocity dispersion profiles (see Figure 3) may signal that FS76 is currently undergoing an interaction with NGC5044 which is at a projected distance of only 30 kpc. The ratio of the mean velocity v_p to the velocity dispersion σ_p can be used as an indicator for the importance of rotation in the flattening of a stellar system. For an isotropic E1 galaxy, flattened by rotation, one expects v_p/σ_p = 0.35. The observed ratio of the peak velocity to the central velocity dispersion is $(v_p/\sigma_p)_{obs}$ = 0.33 ± 0.15, fully consistent with FS76 being an isotropic oblate rotator. Moreover, the best fitting dynamical model shows that the radial velocity dispersion varies only by a few km/s from the equatorial plane towards the rotation axis and therefore pressure differences play only a minor role in flattening this galaxy. Thus, the observed kinematics and detailed dynamical models unambiguously show that FS76 is indeed flattened by rotation and not by pressure. Since these findings were published, more dEs with significant rotation have been discovered, both by us and by others. These results

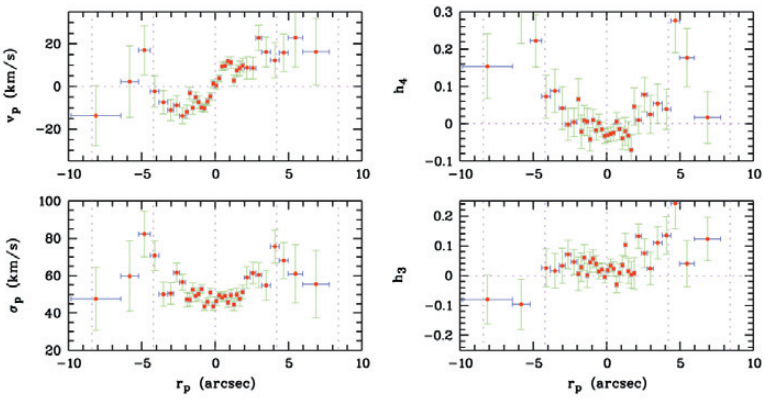

Figure 3: The major-axis kinematics of FS76. Left: mean velocity v_p *and velocity dispersion* σ_p*. Right: Gauss-Hermite coefficients* h_3 *and* h_4*, quantifying asymmetric and symmetric deviations from a Gaussian line-of-sight velocity distribution.*

corroborate the prediction of the harassment scenario that fast-rotating dEs should exist.

dEs with embedded discs

We collected *R* and *I* band images of FCC204 (dE6, M_B=–16.52) and FCC288 (dE7, M_B=–16.18), two Fornax cluster dEs, with FORS2 on Kueyen in November, 2000 (De Rijcke et al. 2003b). Both galaxies have "disky" isophotes, so they are better classified as dwarf lenticular galaxies or dS0s. To check whether this diskiness is caused by the presence of a real stellar disc, we applied an unsharp masking technique. We smoothed the *R*-band image of each galaxy with the MIDAS command filter/med to replace each pixel by the median of a 6″ × 6″ surrounding box. This smoothed image is then subtracted off the original one, highlighting any fine structure. The original and residual images are presented in Figures 4 and 5.

The prominent disc in FCC288 can be traced out to 2 kpc. Clearly visible is the flaring and warping of the disc. The thickness of the disc remains more or less constant around 160 pc inside the inner kpc. Beyond that the disc thickens rapidly, reaching ≈ 500 pc at a radial distance of 2 kpc. FCC204 has a much less impressive disc, traceable to about 1.8 kpc and about 255 pc thick. Besides a large bulge, two brightness maxima at symmetric positions with respect to the nucleus are visible. A possible interpretation is that we are looking edge-on onto a bulge+bar system and that the two brightness enhancements constitute the edges of the bar or perhaps are even small spiral arms.

Spectra of FCC288 and FCC204 were obtained with FORS2 in November, 2000 on Kueyen and November, 2001 on Yepun, respectively. As an example, the major axis kinematics of FCC204 are plotted in Figure 6. Both galaxies are very rapid rotators. Still, they do not rotate fast enough to explain their apparent flattenings. This is most likely due to the fact that the observed kinematics also reflect the motions of the stars that make up the less flattened (i.e. slower rotating, more anisotropic) body of the galaxy. Inside the bulge of FCC204, the LOSVDs have a Gaussian shape. In the discs of both galaxies, the LOSVDs are more peaked and skewed. The edges of what we interpret to be a bar in FCC204 correspond to changes in the velocity dispersion and the rotation velocity. The very fast rotation and the correlation of the various kinematic parameters with the photometric features strengthen our interpretation based on the unsharp masking : both galaxies are seen practically edge-on and contain fast-rotating disc structures. Such embedded stellar discs may be relics from the pre-harassment era, according to the harassment scenario.

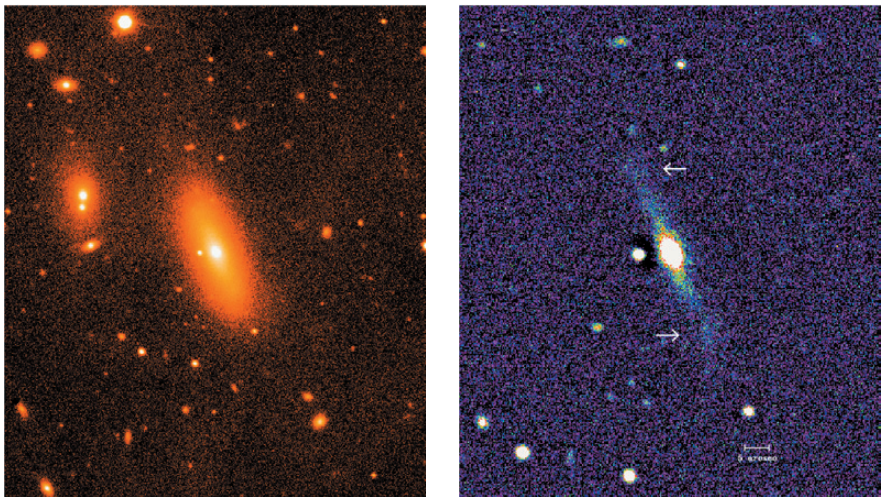

Figure 4: Left panel : 120 sec. R*-band image of FCC204. Right panel : result of unsharp masking. At the outer edges of the disc, two brightness peaks are visible (marked by arrows). North is up, east is to the left.*

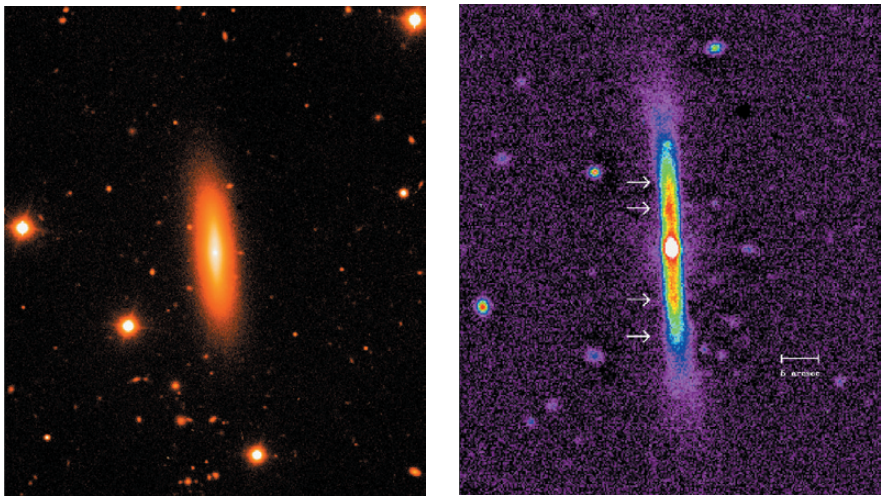

Figure 5: Left panel: 600 sec. R*-band image of FCC288. Right panel: result of unsharp masking. The disc embedded in FCC288 runs practically across the whole face of the galaxy. The flaring of the disc and the brightness fluctuations in it (marked by arrows), which could be spiral arms, are clearly visible. North is up, east is to the left.*

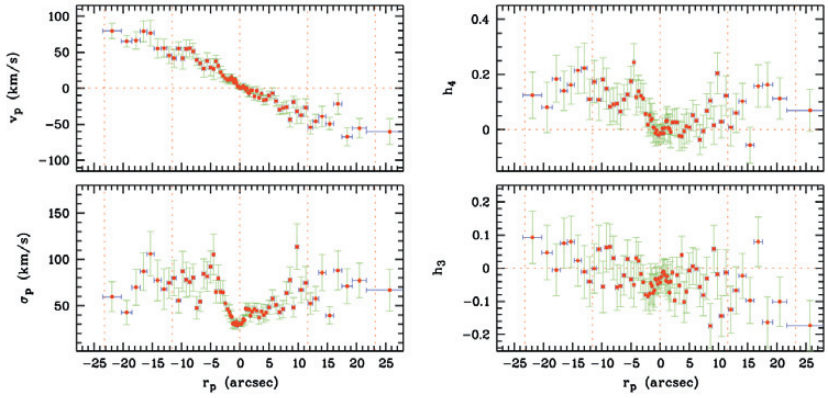

Figure 6: Major axis kinematics of FCC204. Left: mean velocity v_p *and velocity dispersion* σ_p*. Right: Gauss-Hermite coefficients* h_3 *and* h_4*, quantifying asymmetric and symmetric deviations from a Gaussian line-of-sight velocity distribution.*

dEs with a warm ISM

We obtained *B, R*, and *I* broad-band images, Hα+[NII] narrow-band images and spectroscopy of the nucleated dEs FCC046 (dE4N, M_B=–15.29) and FCC207 (dE2N, M_B=–15.09) in the Fornax cluster in November 2000 and November 2001. FCC046 was classified as a non-nucleated dE4 so the presence of its very bright and blue nucleus came as a surprise. The nucleus is resolved under seeing conditions of

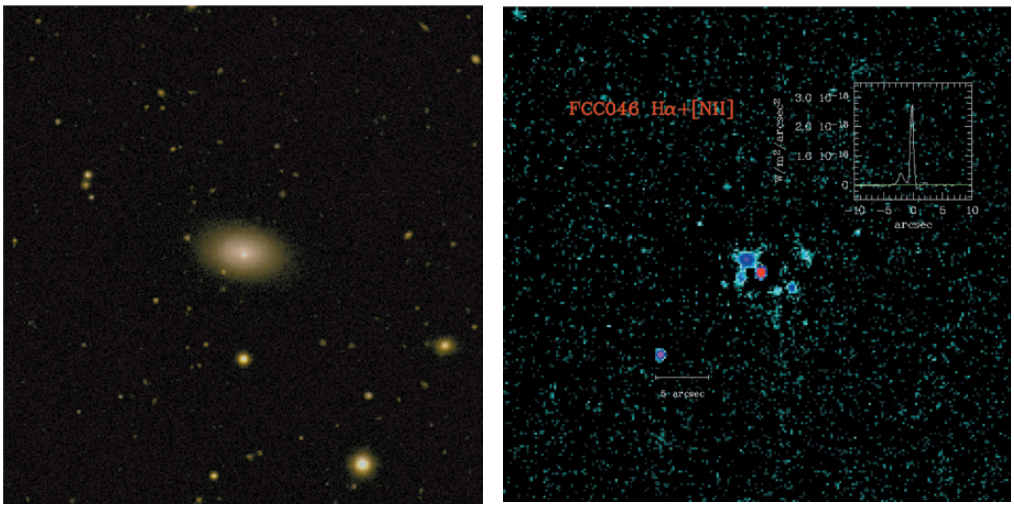

Figure 7: Left panel : a BRI *colour composite image of FCC046. Note the off-centre nucleus. North is up, east is to the left. Right panel : Hα+[NII] emission image of FCC046. Six emission clouds other than the nucleus can be discerned. The horizontal bar measures 5″ on the sky. The inset shows a cut through the central emission region. The intensity is plotted in units of W/m²/arcsec².*

0.8″ FWHM and is offset by 1.1″ to the south-west of the centre of the outer isophotes. It has a blue magnitude m_B = 18.55 mag (M_B=–12.77) and comprises about 10% of the total *B*-band luminosity of the galaxy. FCC046 shows a pronounced lopsided shape. Given that FCC046 is an isolated galaxy in the outskirts of the Fornax cluster, it is unlikely that an encounter caused this asymmetry. Based on broad-band colours, its disturbed shape and its very bright nucleus, FCC046 is akin to the class of amorphous dwarfs, the name coined by Allan Sandage for dwarf galaxies that have a disturbed appearance due to recent star formation and the presence of dust but are not irregular enough to be classified as Im (Magellanic-Cloud type irregulars). The nucleus of FCC207 has a distorted shape: it is more elongated than the bulk of the galaxy (E3 versus E2) and is somewhat kidney-shaped. This is probably due to dust-absorption to the north of the nucleus, noticeable in the *B-R* color map. The *B-R*, *B-I* colors stay essentially constant outside the nucleus. Based on published *UBV* colors and metallicities, it was concluded that FCC207 is too blue in *U-B* (*U-B* = 0.15) and too metal-poor for its *B-V* (*B-V* = 0.78) and this was interpreted as a consequence of the presence of a young stellar population. This motivated us to investigate both objects more closely.

We took 20 minute exposures of FCC046 and FCC207 with the Hα/2500+60 narrow-band filter with FORS2 on Yepun. *R* band images served as off-band images. The narrow-band filter only lets through the light of the Hα 6563 Å emission line of ionised hydrogen and two adjacent emission lines of ionised nitrogen, [NII] 6548, 6583 Å and thus traces the presence of ionised gas. The standard data reduction procedures (bias subtraction, flat-fielding, cosmic removal, interpolation over bad pixels, sky subtraction) were performed with MIDAS. All science images were corrected for atmospheric extinction using the *R* band extinction coefficient and interstellar extinction. The emission-images were converted to physical units (W/m^2) with the aid of the spectrum of a flux-calibration standard star.

Color images and pure Hα+[NII] emission images of FCC046 are presented in Figure 7. The total emission luminosity of FCC046 is L_{em}(FCC046) = 6 ×10^{30} W, about half of which is emitted by the central peak corresponding to the galaxy's nucleus. The total emission luminosity of FCC207 is somewhat higher: L_{em}(FCC207) = 8 ×10^{30} W. The total mass in ionised hydrogen can be estimated assuming complete re-absorption of all Lyman photons and an electron density N_e = 1000 cm^{-3}. We then find that for FCC046 $M_{HII} \approx$ 40–150 $M_\odot$ and for FCC207 $M_{HII} \approx$ 60–190 $M_\odot$, depending on the unknown contribution of the [NII] lines to the Hα+[NII] emission.

In FCC046, the emission is distributed over a bright central region and six fainter clouds, three of which are resolved. The diameters and luminosities of the resolved clouds are consistent with them being supernova-remnants but they are about 10 times larger than HII regions of comparable luminosity. Nebulae around Wolf-Rayet stars could be a plausible alternative and are found in many irregulars and have appropriate luminosities and diameters. The similarities of the broad-band colours of FCC046 to those of star-forming or amorphous dwarfs, its relatively strong core and the presence of emission clouds support the conclusion that FCC046 is actively forming stars, albeit at a very leasurely pace when compared to Blue Compact Dwarfs (BCDs) and amorphous dwarfs which are about a factor 1000 more luminous in Hα. The nuclear emission of FCC046 and FCC207 can be adequately accounted for by photo-ionisation by post-AGB stars although a contribution of Hα emission from star-formation cannot be excluded. Only the emission from the six clouds observed in FCC046 (supernova remants, Wolf-Rayet nebulae) can be interpreted as unambiguous evidence for recent or ongoing star-formation.

Preliminary conclusions

In the course of this Large Program, we have assembled kinematics of unprecedented high quality of a sample of 15 dEs. All data have been reduced and analysed, and the last few objects are being modelled. Outstanding results based on selected objects have been published or are in press. More papers, in which we will present our conclusions based on the photometry, dynamics, and line-strengths of the full sample, will be submitted shortly.

Thanks to the high spatial and spectral resolution of our observations, we have uncovered the existence of dEs with complex behavior and internal structures (such as embedded stellar discs) that are hard to fit into a simple scenario in which dEs form through the collapse of primordial density fluctuations, like the wind model. Clearly, dEs are anything but small "island universes" that evolve in splendid isolation: their evolution appears determined, at least in part, by their environment. Thus, the harassment scenario offers an attractive explanation for many observed features that are hard to explain with the wind model.

References

De Rijcke S., Dejonghe H., Zeilinger W. W., Hau G. K. T., 2001, *ApJL*, **559**, L21-L24
De Rijcke S., Zeilinger W. W., Dejonghe H., Hau G. K. T., 2003, *MNRAS*, **339**, 225-234
De Rijcke S., Dejonghe H., Zeilinger W. W., Hau G. K. T., 2003, *A&A*, **400**, 119-125
Ferguson H. C., Binggeli B., *A&ARv*, **6**, 67-122
Moore B., Katz N, Lake G., Dressler A., Oemler Jr. A., *Nature*, **379**, 613-616
Mori M., Yoshii Y., Tsujimoto T., Nomoto K., *ApJL*, **478**, L21-L24
Simien F., Prugniel P., *A&A*, **384**, 371-382